REPORT DOCUMENTATION PAGE

Form Approved OMB NO. 0704-0188

1. REPORT DATE (DD-MM-YYYY)	2. REPORT TYPE	3. DATES COVERED (From - To)
18-06-2008	Technical Report	1-Jun-2004 - 31-Mar-2008

4. TITLE AND SUBTITLE
DIAGNOSTICS OF 3D DYNAMIC STALL ON ROTOR BLADES

5a. CONTRACT NUMBER
W911NF-04-1-0184

5b. GRANT NUMBER

5c. PROGRAM ELEMENT NUMBER
611102

6. AUTHORS
Kevin Watson, Jason Cormey, Narayanan Komerath, James DiOttavio

5d. PROJECT NUMBER

5e. TASK NUMBER

5f. WORK UNIT NUMBER

7. PERFORMING ORGANIZATION NAMES AND ADDRESSES
Georgia Institute of Technology
Office Of Contract Administration
Program Initiation Division
Atlanta, GA 30332 -0420

8. PERFORMING ORGANIZATION REPORT NUMBER

9. SPONSORING/MONITORING AGENCY NAME(S) AND ADDRESS(ES)
U.S. Army Research Office
P.O. Box 12211
Research Triangle Park, NC 27709-2211

10. SPONSOR/MONITOR'S ACRONYM(S)
ARO

11. SPONSOR/MONITOR'S REPORT NUMBER(S)
46454-EG.1

12. DISTRIBUTION AVAILIBILITY STATEMENT
Approved for Public Release; Distribution Unlimited

13. SUPPLEMENTARY NOTES
The views, opinions and/or findings contained in this report are those of the author(s) and should not contrued as an official Department of the Army position, policy or decision, unless so designated by other documentation.

14. ABSTRACT
This project investigated the nature of the velocity field behind the separation line in dynamic stall on rotor blades, particularly the centrifugal effects and radial velocity field. Initial experiments were performed using a single-bladed rotor in hover with transient stall induced by an inflow obstructor. A 2-bladed teetering rotor setup was then constructed in the Georgia Tech 7' x 9' tunnel. PIV measurements confirmed the finding of discrete quasi-periodic streamwise vortical structures in the radial flow behind the separation line in both experiments. Co-rotating structures suggest that the free shear layer formed at stall rolls up into discrete cells. The spanwise spacing of structures is approximately the height of the separated flow region. The presence

15. SUBJECT TERMS
3D dynamic stall, PIV, vortical structures

16. SECURITY CLASSIFICATION OF:			17. LIMITATION OF ABSTRACT	15. NUMBER OF PAGES	19a. NAME OF RESPONSIBLE PERSON
a. REPORT	b. ABSTRACT	c. THIS PAGE			Narayanan Komerath
U	U	U	SAR		19b. TELEPHONE NUMBER 404-894-3017

Report Title

DIAGNOSTICS OF 3D DYNAMIC STALL ON ROTOR BLADES

ABSTRACT

This project investigated the nature of the velocity field behind the separation line in dynamic stall on rotor blades, particularly the centrifugal effects and radial velocity field. Initial experiments were performed using a single-bladed rotor in hover with transient stall induced by an inflow obstructor. A 2-bladed teetering rotor setup was then constructed in the Georgia Tech 7' x 9' tunnel. PIV measurements confirmed the finding of discrete quasi-periodic streamwise vortical structures in the radial flow behind the separation line in both experiments. Co-rotating structures suggest that the free shear layer formed at stall rolls up into discrete cells. The spanwise spacing of structures is approximately the height of the separated flow region. The presence of these structures helps explain the nature of the radial flow variation from root to tip in the separated flow region. Measurements of the variance in the radial velocity profile suggest that the breakup into discrete structures originates in the region of radial acceleration rather than at the outer edge of the separated flow.

DIAGNOSTICS OF 3D DYNAMIC STALL ON ROTOR BLADES

Narayanan Komerath, Jim Di Ottavio, Kevin Watson, Jason Cormey

Final Progress Report on ARO Project W911NF0410184, Georgia Tech project 1606W71, through March 2008.

FOREWORD

This report is being submitted at the end of 3.5 years into the project. It has succeeded in capturing several features of the radial flow in the separated flow region on a rotor blade in transient or dynamic stall. It has succeeded in two different experiments. The first was conducted in a hover facility where stall was induced by reducing the inflow using an inflow obstructor plate, and thus boosting the instantaneous angle of attack well beyond stall. In the second experiment, a two-bladed teetering rotor was operated under dynamic stall conditions in a wind tunnel, with collective and and cyclic pitch adjusted to get into dynamic stall conditions.

The measurements reported here focus on the zone above the blade when it is in the 270 degree azimuth region (retreating blade side). Continuing work explores what happens at other azimuths, and pursues the findings in this report.

TABLE OF CONTENTS

STATEMENT OF THE PROBLEM STUDIED

Introduction

Retreating-blade stall on helicopter blades involves strong radial acceleration in the boundary layer, spanwise velocity, and turbulent boundary layers upstream of separation. This project studies the 3-dimensional aspects of retreating blade stall using a progression of experiments.

Development of hub-mountable instrumentation has proceeded, enabling laser velocimetry where the counter processor is replaced by software in a small computer. The computer has survived 200rpm while operating. The second phase forward flight dynamic stall experiment, using a 2-bladed teetering rotor in the John J. Harper wind tunnel, became operational during this past year. This Results section first describes the new experimental facility and then summarizes the results and conclusions obtained. These are being prepared for submission in AIAA papers over the upcoming year.

Project Objectives

The long-term objectives of this research are:

1. Detailed mechanisms of retreating-blade stall on a helicopter rotor blade.
2. Free shear layer interactions related to the operation of leading-edge and trailing-edge devices on rotating blades.
3. Temporal evolution of flows and flow interactions relevant to active-control of separation and vortex interactions.

Synopsis of Previous Years

During the first two years, we made substantial progress in developing facilities where hub-mounted diagnostics could be applied in future, and towards developing diagnostic instrumentation suited to that purpose. Having pushed that as far as present miniaturization of certain key components would allow, we focused on the fluid dynamics of the radial flow over rotor blades, behind the separation line in dynamic stall. This represents a largely unknown area in the research literature on dynamic stall related to helicopters (and to wind turbines).

SUMMARY OF RESULTS

1. Hub-mounted data acquisition

Two laptop computers small enough to be mounted on a 6” diameter rotor hub (Sony VAIO, micro laptop PC) were acquired. These could be operated on a rotating table at up to 200 rpm; however hard disc operation was intermittent because of acceleration-sensitive protection

mechanisms. The entire data acquisition software could be placed on USB flash drives; however, system startup from these drives was not possible on the existing operating systems. The basic idea of operating with COTS hardware of this class was shown to be feasible. Communication with a device in the laboratory reference frame using wireless was also occurring, so that in principle, such a device could be commanded from a laboratory computer to start and stop data acquisition. Runs would have to be limited to the time available before the USB drives ran out of space, but with 2GB and 4GB drives, this is also not a major issue.

2. Software-Based Counter Processor for Hub-Mounted Laser Velocimeter

A counter-type processor of LV signals was successfully implemented in software and demonstrated using the micro-laptop PC to be used on the rotor hub. The counter was shown to work in the Megahertz regime, needed for LV in the rotor application, using a signal generator. Tests with a rotating disc have also been commenced. Two difficulties with integrating this velocimeter with a rotating dynamic-stall experiment are:
a) the frequency shifter power supply and opto-electronics on this system are not robust enough to survive vibration, nor are they miniaturized.
b) the vibration level on our forward flight rotor setup during dynamic stall is not yet low enough to try this integration, even without the frequency shifting.

3. Pressure-Sensitive Paint Studies

The pressure-sensitive paint studies have led to a peer-reviewed publication on high-response PSP. In the field of PSP, there are at least two frontiers: sensitivity and frequency response. The chemical requirements and surface preparation for each are quite different at present. and different paint formulations and surface textures are used. We pursued an opportunity for a breakthrough in the frequency response arena: collaborating with Dr. Jim Gregory, then a PhD candidate in Prof, Sullivan's group at Purdue, to perform clean controlled experiments capturing the complex mode shape of a higher-order mode in an acoustic resonator. We have thus participated in pushing the frequency response frontier past 1600 Hz. The sensitivity frontier is still some distance away from reaching where we can use PSP in our present experiment, given the low rpm used. These experiments and results are described in a paper in the Journal of Sound and Vibration [1].

4. Inflow Obstructor Experiment

Unlike laser Doppler velocimetry, where time-resolved velocity at a single point can be obtained in the blade-fixed reference frame, there is no advantage to using Particle Image Velocimetry in the blade-fixed frame. The time between two successive velocity fields achievable with our systems is on the order of 30 milliseconds, at least one order of magnitude away from what can be achieved with LDV. So as the first stage of our long-term effort, we focused on using PIV. This was to look at the fluid mechanics of the radial flow over a rotor blade under transient stall conditions such as those encountered in dynamic stall. This followed the plan originally

proposed. The progress towards the first objective, that of studying the radial flow in dynamic stall, is discussed in detail below.

A triangular metal plate was used to cover a 60-degree sector of the inflow to a single-bladed NACA 0012 rotor blade in the Georgia Tech 9-foot Rotor Flow Diagnostics Facility. This work is detailed in AIAA Paper 2006-3377, Reference [2]. Conclusions from the inflow obstructor experiment are summarized below.

1. A single-blade hover facility was used with an Inflow Obstructor plate to simulate the dynamic stall region downstream of the separation line.
2. PLIS and PIV validate that stall indeed occurs, based on stoppage of the through-flow.
3. Downstream of the stall line, the radial velocity along the blade develops an outward direction. Stall cells formed along the radius exchange fluid away from the boundary layer.
4. The phase-locked radial velocity profile shows higher deceleration of radial out-flow from leading edge to chord-wise location where flow recirculation begins. This suggests that the inboard directed velocity of the upper surface flow dominates over the centrifugal effect, from the leading edge to separation point. Beyond separation, centrifugal flow dominates.
5. The cells of radial flow separation, while comparable in scale to the blade chord, vary from cycle to cycle.

Figure 0: Dynamic Stall rig assembly in the test section of the John J. Harper wind tunnel

Thus the first experiment used a modified hover setup where the inflow is interrupted over a selected sector to trigger transient inboard flow separation. This succeeded in demonstrating that a repeatable stall event was induced, in order to develop diagnostic concepts without the complexities of a forward-flight rotor setup. The interesting fluid dynamics result seen there is that the radial flow rolls up into vortical structures, whose axes are aligned roughly along the blade chord. These features prevent discrete filaments of fluid from remaining in the highly accelerated blade boundary layer, and thus mitigate the centrifugal pumping effects.

5. High Advance Ratio Facility Design

After reviewing options for designing a dynamic stall forward flight experiment rig, a teetering hub design was selected. This was to remove the need to “fly” the rotor to its operating condition, and instead be able to start the rotor and then the wind tunnel, and independently reach operating points. Fully articulated rotors would require “flying”

from the control room to avoid encountering disastrous conditions on the way to the operating point.

Table 0: Rotor Rig Parameters

ROTOR SPECIFICATIONS		
Blade Mass Total	1.752	**kg**
Blade Span	0.62	**m**
Blade Chord	0.178	**m**
Disc Radius	0.886	**m**
Solidity	0.0895	
Precone	1.6	**deg**
Max Collective	10	**deg**
Max Cyclic	6.5	**deg**
Max TPP Tilt	16	**deg**
Airfoil	NACA 0012	
Blade Aspect Ratio	3.49	
Motor HP	5	
Height	1.575	**m**

Since the setup is intended for aerodynamic/ flow diagnostic tests, blade elasticity is not an issue. We selected a 600 lb gross weight personal helicopter kit as the basis of the design. The main and tail rotor hubs and swashplates, as well as two NACA 0012 main rotor blades were acquired. The original rotor blades were 6.55m in diameter, and designed to operate at around 450 rpm. Thus the hub is built to take the centrifugal load under such conditions, and support over 2700N (600 lb) thrust in climb. One blade was cut to produce two blades for our setup, each 0.62m in span. Clearly the hub is safe for the present experiment operating range of.00 to 500 rpm. Pitch links were strengthened for the dynamic stall rig (Fig. 1). Facility parameters are in Table 1.

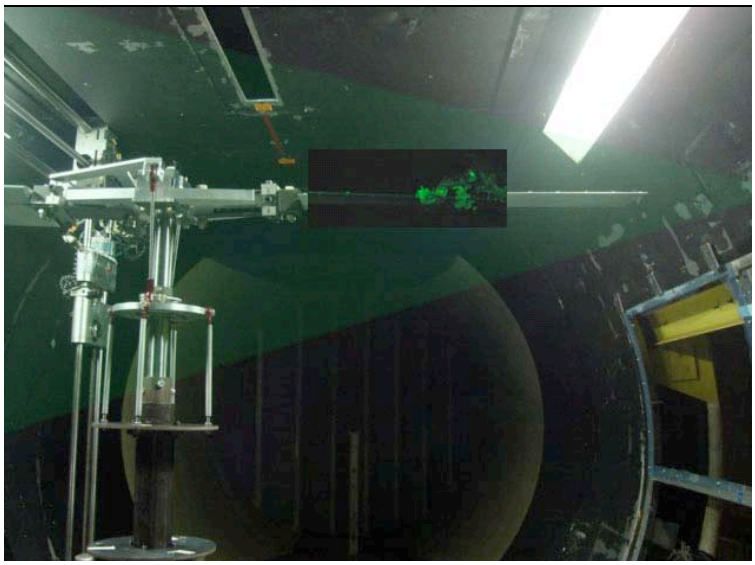

Figure 2: Flow image superposed on blade image

The viewing plane used for flow visualization and PIV is shown schematically on a picture of the Retreating Blade Side (RBS) or the rotor in Figure 2. The camera is mounted upstream of, and below the 270 degrees azimuth. Operating conditions were selected by trial and error, varying collective and cyclic at selected advance ratio to verify the occurrence of dynamic stall. At 10 degrees collective and 5 deg. cyclic, the effective angle of attack at 270 degrees was calculated to be 18.6 deg., and flow visualization of the chordwise flowfield using mineral oil fog and a pulsed laser sheet, verified stall over most of the blade at mid-radius. The image in Figure 2 suggests vortical structures in the stalled flow as the trailing edge of the blade passes the measurement plane.

Figure 3 shows a sample velocity vector plot from instantaneous PIV data (100 microseconds between images), taken about 1 mm downstream of the trailing edge in the vertical/radial plane at 270 degrees rotor azimuth. There are clearly discrete zones of radial flow, though now there is

no actual upflow in the trailing edge plane, unlike the case with the inflow-obstructor experiment. Four oval-shaped regions are marked to indicate the discrete zones. Sampling of numerous such flowfield results showed that the number of discrete zones in the viewing plane was approximately 4 on average, i.e., the spacing between the structures was roughly constant. This spacing worked out to be roughly the same as the nominal height of the separated flow region at the trailing edge of the blade, suggesting discrete vortical structures occupying the stalled region. The average structure diameter is 0.033m, while the height of separated flow region is 0.035 to 0.045m, calculated by assuming that separation occurs at the maximum thickness part of the blade at the given inclination angle. This lends credence to an approximate model of the dynamic stall flowfield as shown in Figure 4, where the separating shear layer rolls

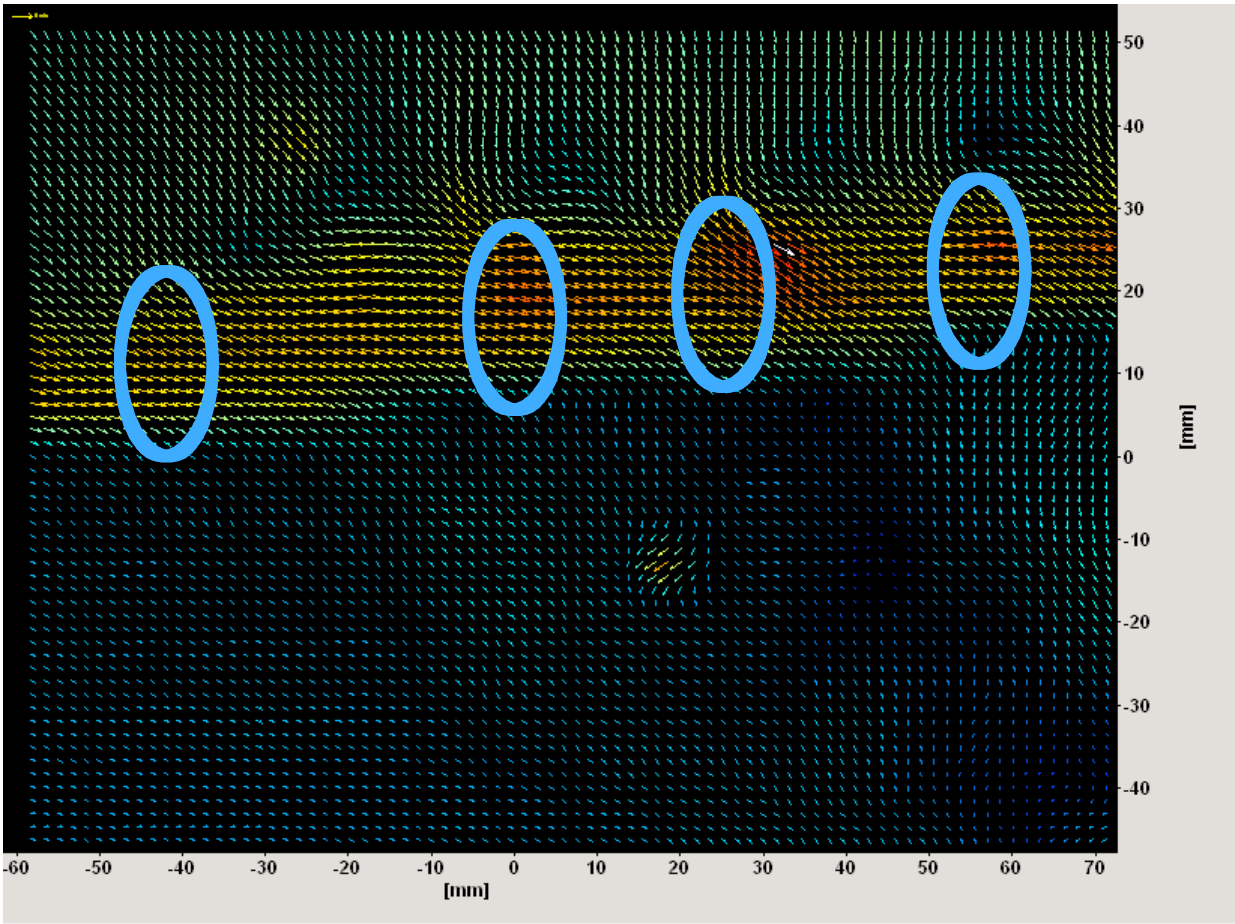

Figure 3: Velocity vectors in an axial-radial plane 1mm behind blade trailing edge at 270 deg. azimuth. 100 microseconds delay between PIV images. Red is highest magnitude.

into discrete structures that grow with downstream distance. To-date we have only succeeded in measuring these at the plane 1mm behind the trailing edge; current efforts focus on moving up the chord towards the point of separation. The difficulty has been that we had to change lasers and cameras in a troubleshooting sequence, and these resulted in the laser sheet coming from below the rotor plane – the flowfield above is in shadow. Currently we have aligned our original laser system to capture the flow above the blade.

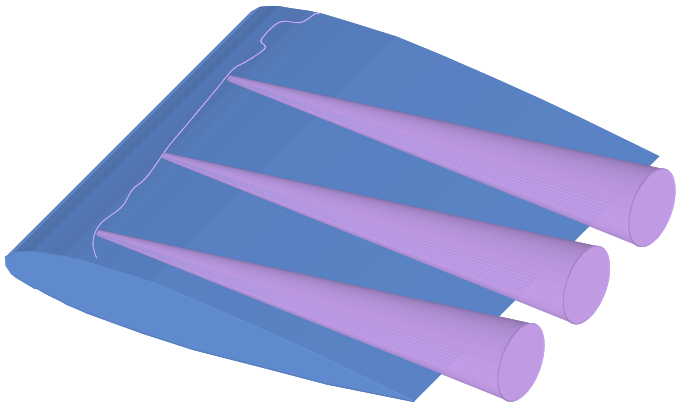

Figure 4: Schematic representation of discrete stall structures.

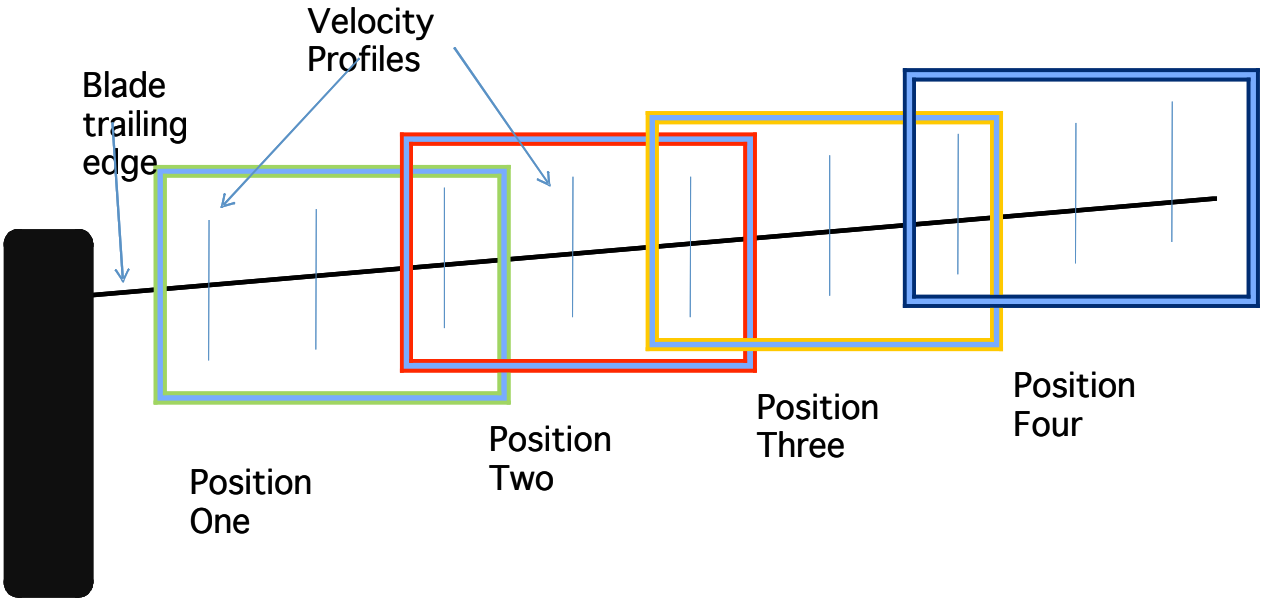

Figure 5: PIV windows along the blade trailing edge at 270 degrees azimuth.

The PIV window was moved in steps along the blade radius, and 100 image-pairs were captured at each position. The locations of these windows are shown in Fig. 5. The windows overlapped. To examine the radial velocity, three vertical lines were chosen in each window as shown. The radial velocity profile from individual (instantaneous, 100 microsecond) velocity fields was extracted along each vertical line. Figure 6 shows a sample.

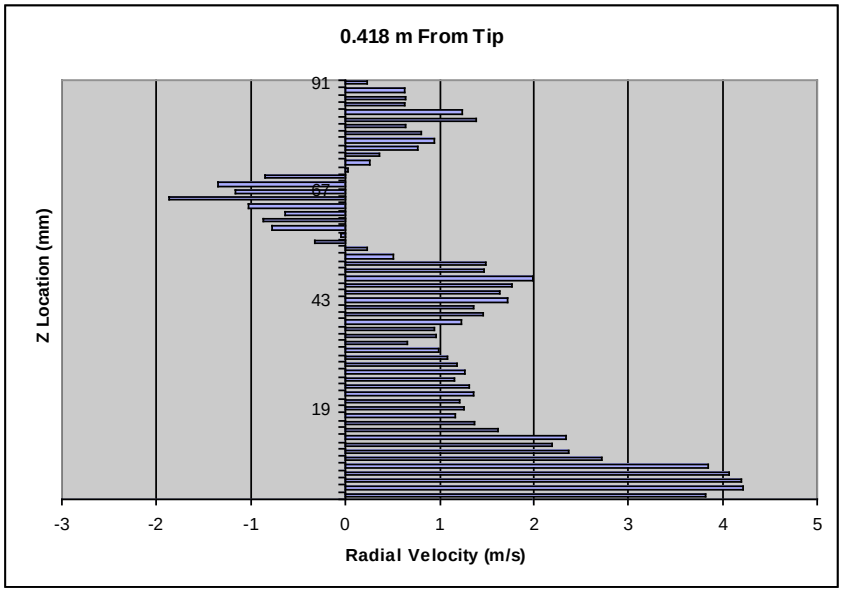

Figure 6: Profile of radial velocity at r/R=0.528, immediately behind the trailing edge at 270 deg. azimuth

Figure 6 shows the velocity profile at 0.418m from the tip, which corresponds to r/R= 0.528 for the rotor radius of 0.886m. The vertical axis is the distance along the vertical (i.e., parallel to the rotor axis), and the range shown corresponds to $\Delta z/R$ of 0.102, or a $\Delta z/c = 0.51$, for the blade chord of 0.178m. This is less than the height of the separated flow region, which is approximately 0.15 to 0.2R above the trailing edge. The bottom of the vertical axis is the blade trailing edge location. We see that the viscous boundary layer under the radial flow appears to have been partially captured. Above this thin region, the radial velocity profile reaches a peak, and then falls off. These features are qualitatively repeatable in all the images; however, the velocity field features above this region are not consistent from image to image. This is understandable for a separated flow region.

Figure 7 shows the profile at r/R = 0.643, and Figure 8 shows it at r/R = 0.758. The peak radial velocity is lower than that at the more inboard location. This is attributable to the formation of the stall cells that exchange the radial flowing fluid away from the blade surface, and to the fact that the tip region is not stalled. Thus the chordwise extent of stall may be expected to be smaller as one moves outboard.

At r/R=0.93, the tip vortex influence dominates. Figure 9 captures the tip vortex velocity field. At this condition, the tip vortex has a core diameter of approximately 0.16c, (or 1.33 times thickness), comparable to the expected 0.12c, if the core is the same size as the thickness of the airfoil. The center of the tip vortex is approximately at this location, as seen from Figure 10. However, the point is that the tip vortex is still fairly strong, indicating positive lift generation in the outboard region, whereas the inboard region is stalled. Again, substantial differences occur from one velocity field to another at the same blade azimuth (not shown here), above the radial flow region. This is to be expected, since it is a separated flowfield.

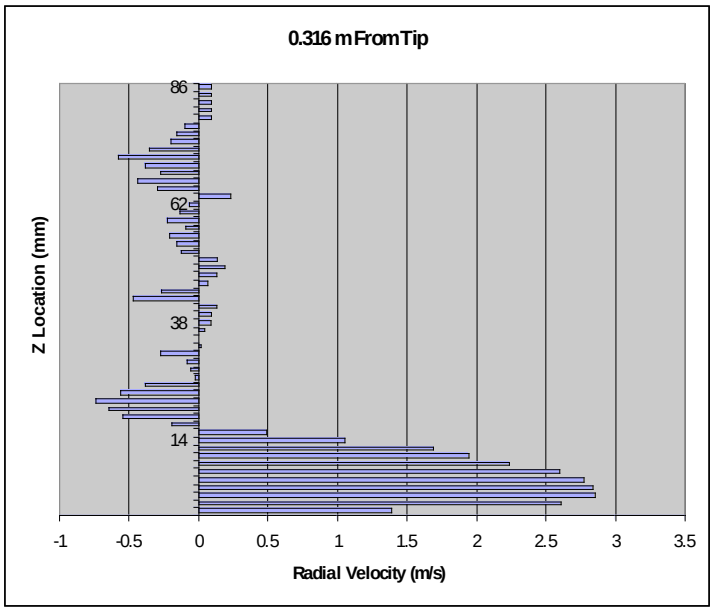

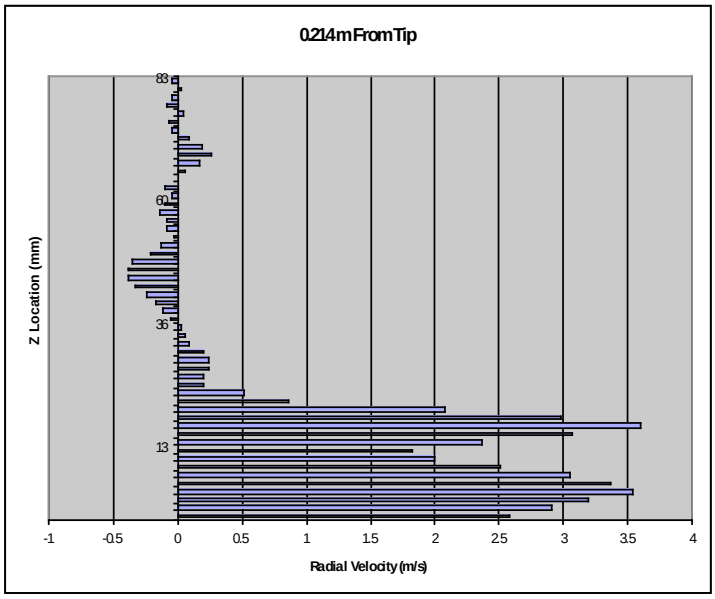

Figures 7(above) and 8 (below): Profiles of radial velocity at r/R=0.64 (Fig.7) and 0.758 (Fig.8), immediately behind the trailing edge at 270 deg. azimuth

Fluctuation Levels

Mean and root mean square (RMS) radial velocity profiles were created by analyzing velocity data from the same spatial regions from 100 separate velocity fields acquired at the same rotor azimuth. The goal here was to test hypotheses regarding where the discrete cells originated. In other words, if the rms fluctuation levels were higher in the region near the external flow, then one could surmise that the discrete cells originate from the shear layer between the external flow and the separated region. On the other hand, if the fluctuations are higher nearer the wall, where the radial flow is strong, then one could surmise that the cells are driven by the radial flow. Thus we could gain a preliminary understanding of whether the radial flow is a stabilizing or destabilizing feature of the flowfield. A MATLAB code was created to assist in averaging and RMS calculations of the 100 image pairs and creating the velocity profiles. The code also normalized the vertical axis so that the trailing edge of the blade would be at a height of zero. Two mean and RMS radial profiles can be seen in Figure 11.

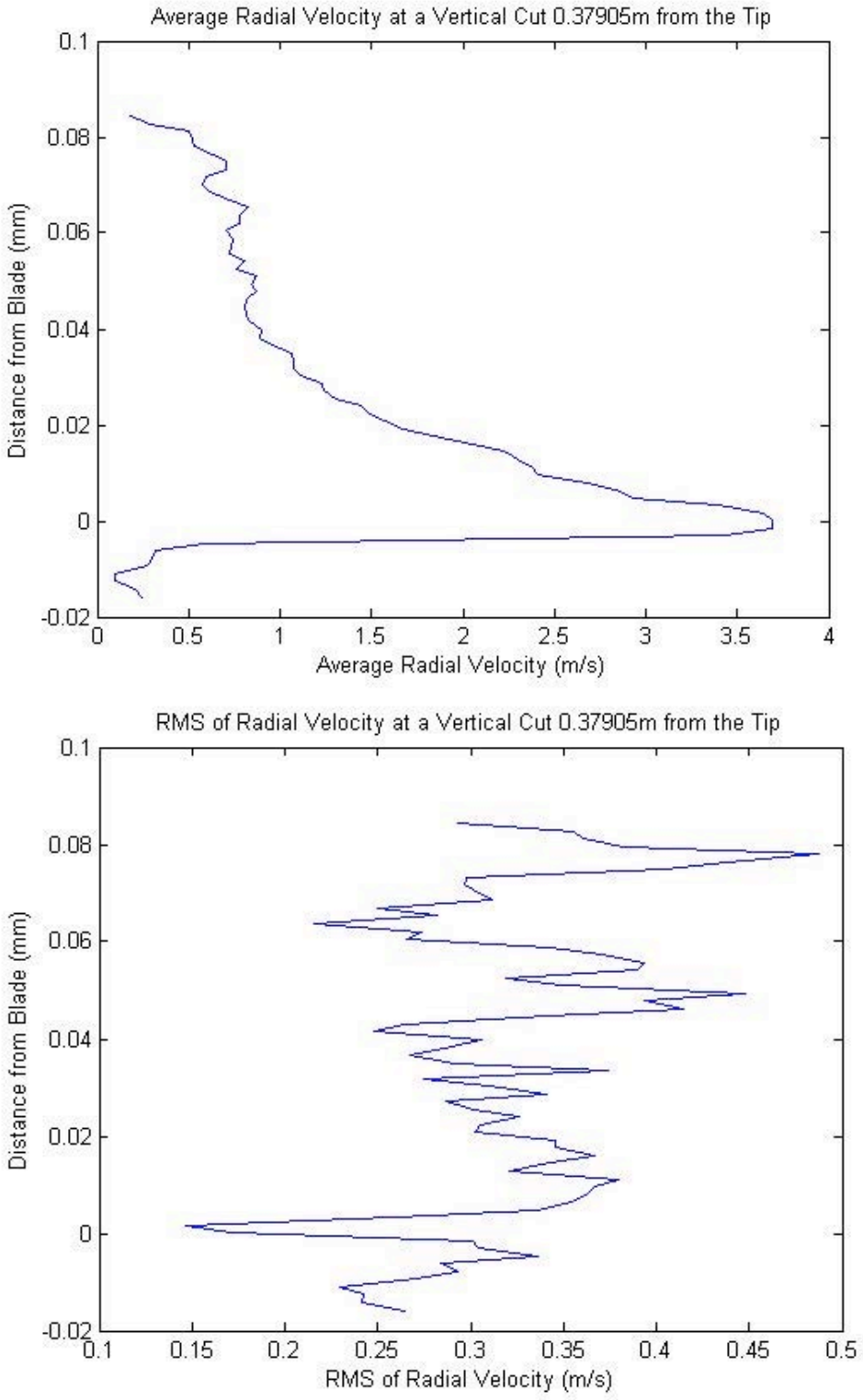

Figure 10: PLSI flow image of the tip vortex, showing the center at 11mm from the tip.

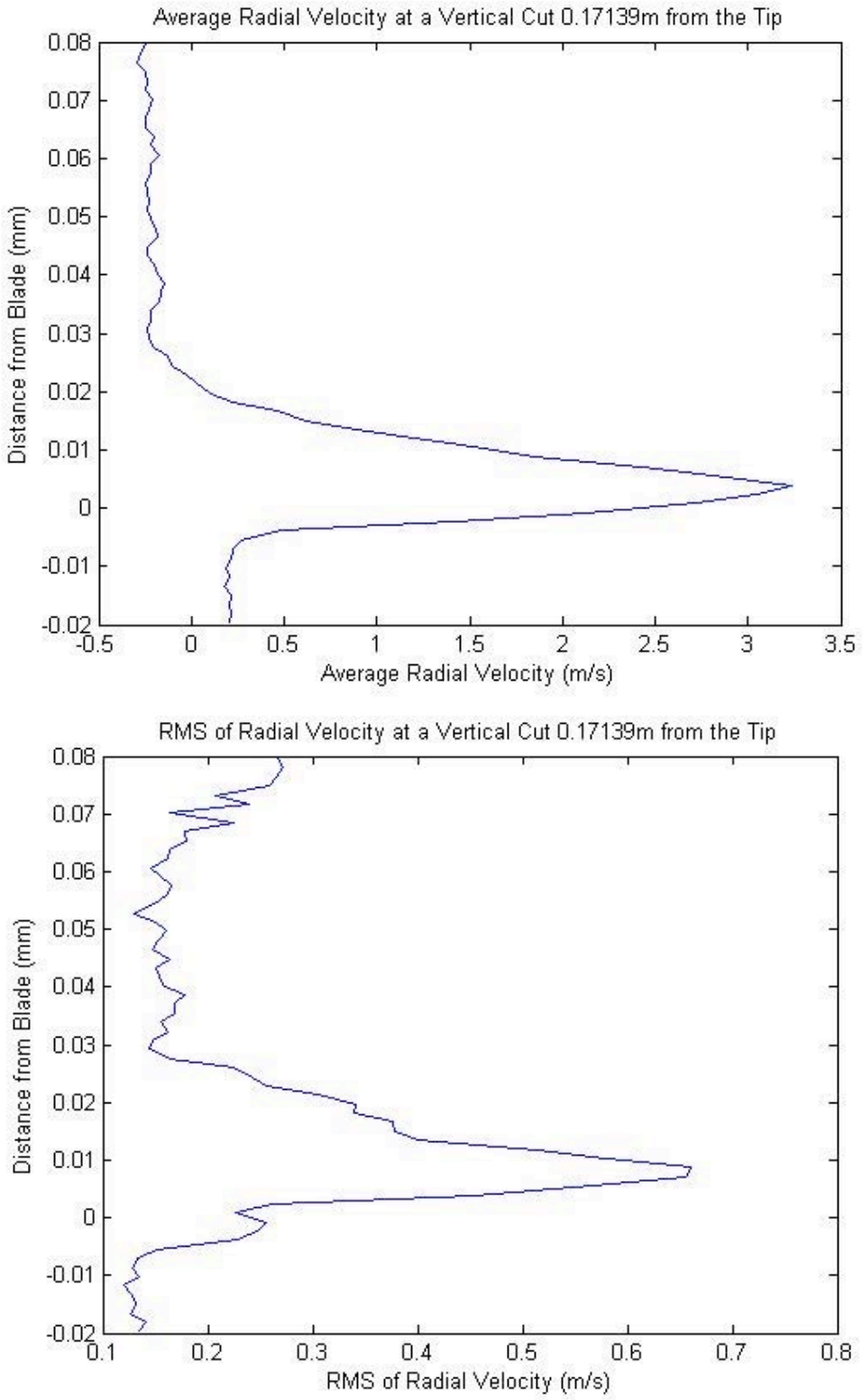

Figure 11 : Mean and RMS Radial Velocity Profiles at r/R=0.586 and r/R=0.814

None of the cells appeared in the mean velocity profiles suggesting that these structures were always in different locations. Similar to the instantaneous radial velocity profiles, the radial velocity peaked close to the surface of the blade and decreased as the positions moved outboard.

Again, positive radial velocity is flow moving outboard. The inboard RMS profiles suggest that the radial flow has a stabilizing influence as the RMS fluctuations are well above the surface of the blade. However, as one moves outboard towards the tip but still outside of the tip vortex influence, the RMS peak is at the surface which suggests the radial flow is a driver of instability. An example of these two different RMS profiles can be seen in Figure 11. The RMS data does not show distinct trends from inboard to outboard locations. Data at other positions fall in between the two understandable results.

Discussion of Trailing Edge Results

Similar structures to those observed in this wind tunnel experimentation were seen in the inflow obstructer cases earlier. These structures seem to be formed by the free shear layer formed at stall rolling into columns or cells. Unlike the inflow obstructer experiment, no upward flow was observed. Furthermore, these cells seem to be located within the separated region, which leads to the assumption that they are forming at the point of separation. The spacing, although initially thought to be equal to the height of the separated region, cannot be clearly determined as the number of cells and the cells height above the surface vary greatly from image to image.

The radial velocity profiles that were created show strong radial outflow at inboard portions of the blade. As images moved outboard, the radial outflow decreased. This supports work done by Yang and colleagues[11] that concludes that centrifugal flow is dominating over the inboard inflow at the trailing edge. Additionally, the tip vortex measurements correspond to the theory that there is deep stall inboard and weaker stall near the tip. This suggests that the stall line will move towards the trailing edge as one moves outboard as shown in Figure 12. These radial velocity profiles were repeatable near the surface of the blade. This cannot be said for velocities above the separated region. This discrepancy could be due to vector errors near the edges of the image frame or a lack of seeded flow that far above the surface.

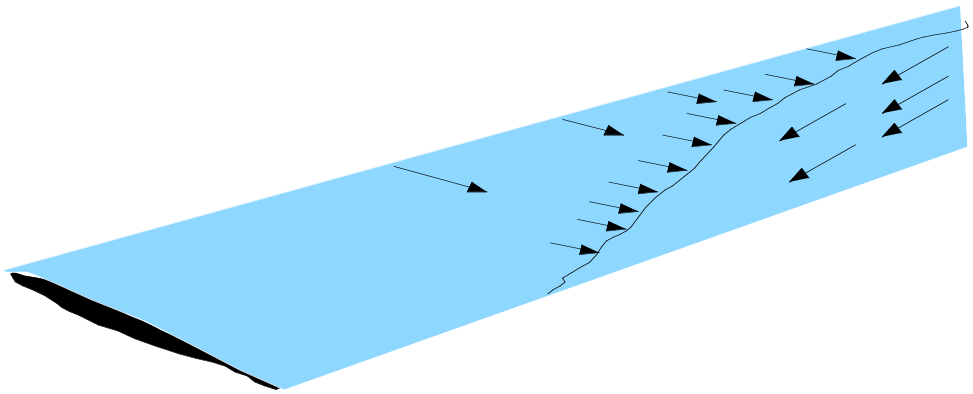

Figure 12 : Radial Flow and Separation Line on a Rotor Blade

Velocity in cross-flow planes at other chordwise stations

It was decided that 12 image positions were to be taken. Of the four spanwise positions as shown in Figure 5, position four would not be included because of the strong tip vortex influence on the flow in that image. For the three remaining positions, four chordwise positions would be measured. In addition to the trailing edge, measurements would occur at 2, 4, and 6 inches from the leading edge. The locations of these 12 positions are highlighted in Figure 13.

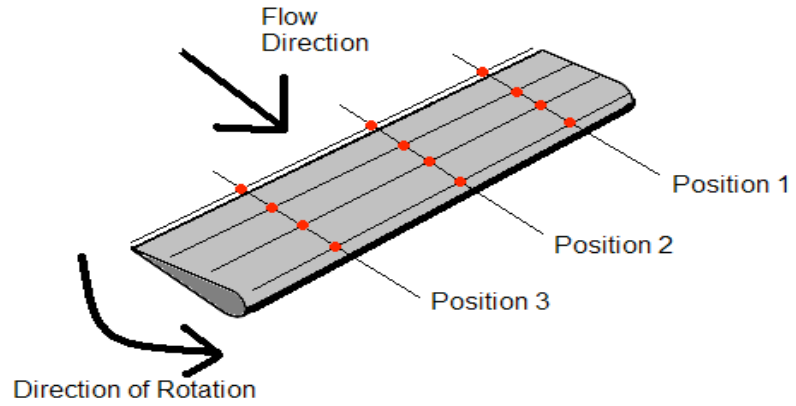

Figure 13 : Chordwise Image Positions

One hundred image pairs were again taken at each location. The cross-correlation procedure including image post-processing did not change from the trailing edge experiments. Additionally, the operating conditions of the rotor and wind tunnel remained at 200 RPM and 20 ft/s respectively. An instantaneous velocity vector at x/c=0.429 is shown in Figure 14.

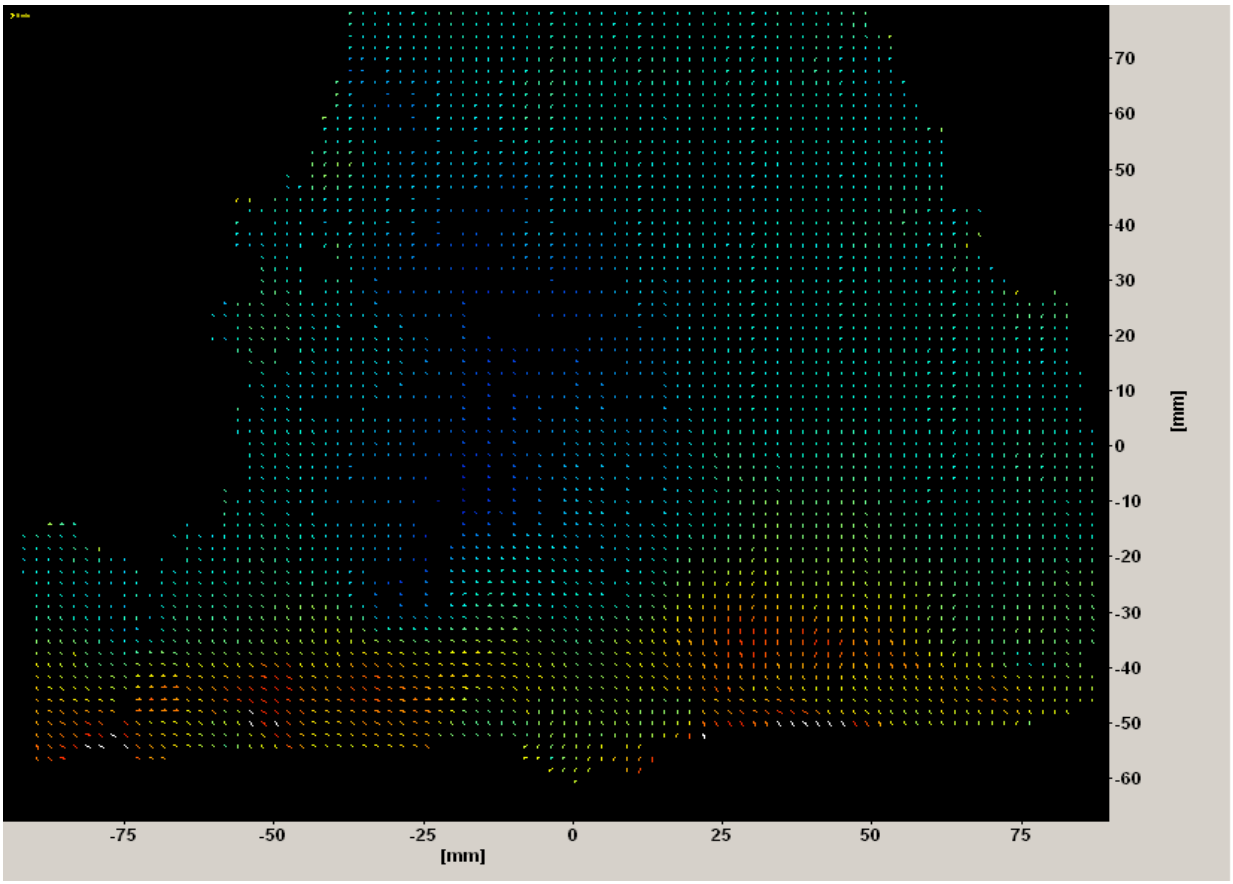

Figure 14 : Chordwise Instantaneous Velocity Vectors at x/c=0.429

The images were scaled to the same dimensions. They were scaled in such a way to properly show the increasing magnitude of the velocity vectors. It can be clearly seen that the discrete structures are again appearing, as was the case for the trailing edge measurements. However, because of the scaling, the cells are harder to see in the trailing edge images (x/c=1). There are no cells seen in the images which correspond to x/c=0.143. It should be noted that this chordwise position is forward of the separation point.

Some initial qualitative observations can be made at this point. It is assumed that the separation point is occurring at the point of maximum thickness, which for the case of this NACA 0012 blade is at about 30% chord, or 4.9 inches from the trailing edge. Therefore, the first three images of an image position (x/c=1, x/c=0.714, and x/c=0.429) are within this separation region while the last image (x/c=0.143) falls outside. The cell structures are seen within the first three images of a position and are observed to gain strength and move closer to the surface of the blade as the image locations approach the separation point. This supports the theory that these cells are formed at the separation point and stay within the separation region. The separation region is expected to become smaller as one approaches the separation point. The magnitude of the vectors above the separation region are decreasing as the images approach and pass the separation point suggesting a decrease in inflow.

As was done with the trailing edge measurements, mean and RMS radial velocity profiles were created for each chordwise location. These profiles look similar to the trailing edge cases.

As with the trailing edge experiments, no cell structures appeared in the mean velocity profiles. It can be said then that the discrete structures are always in different locations along the blade. The radial velocity was seen to again peak close to the blade surface and decrease as positions moved outboard. This was shown for trailing edge measurements and now can be seen to be true at each chordwise location as well. This spanwise trend can be easily seen in Figure 15. This strengthens the theory that deep stall is occurring inboard and getting weaker as measurements approach the tip.

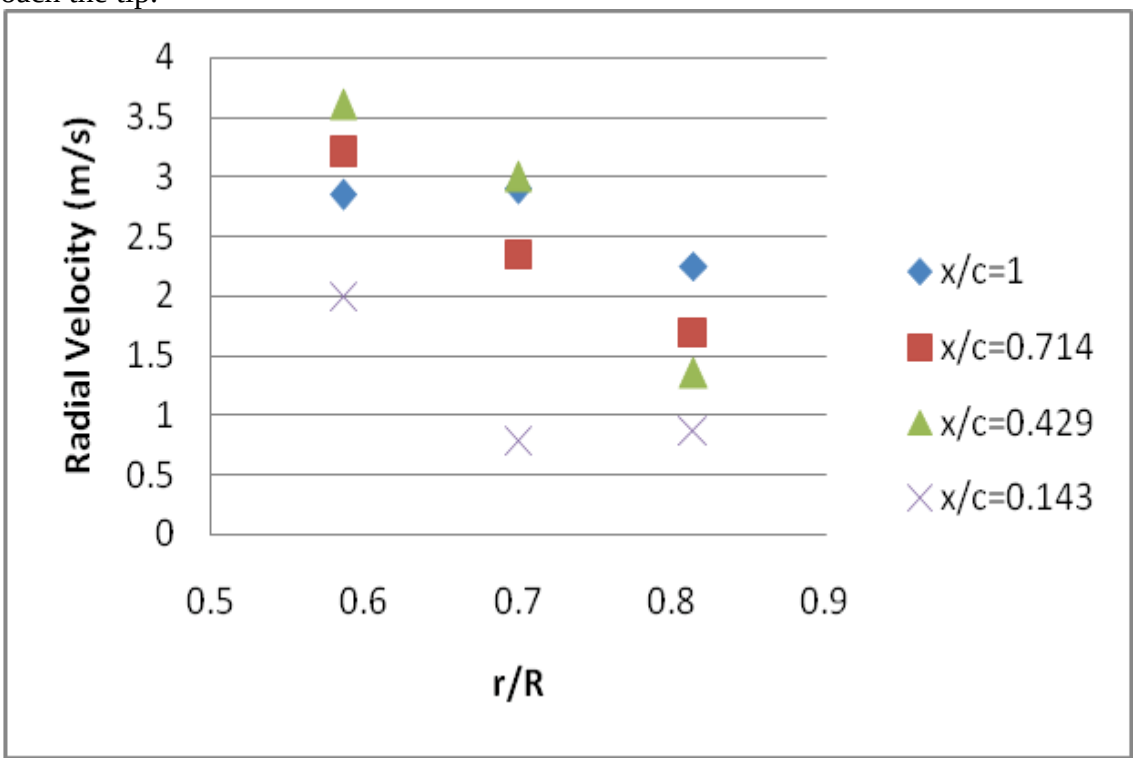

Figure 15 : Radial Velocity vs. Spanwise Location

When examining for chordwise trends, it was less clear that there was any decreasing or increasing tendencies. This chordwise plot can be seen in Figure 16. If more chordwise positions were explored it is believed that for each position, the radial velocity would remain fairly constant along the chord until the separation point. The interesting thing to point out from Figure 16 is what occurs forward of the separation point. The separation point on the NACA 0012 airfoil is assumed to occur at x/c=0.3. After this point, the positive radial velocity indicates outward radial flow and domination by the centrifugal effect. Forward of the separation point, the radial velocity begins to decrease as the inboard-directed inflow begins to dominate the flow. At x/c=0.143 radial velocity goes negative, indicating inboard flow, at about 20mm above the surface of the blade and remains slightly negative above that point. It is believed that if another chordwise position was measured beyond x/c=0.143, these negative radial velocities would be observed on the blade surface in the mean radial velocity profiles. This conclusion is supported by Yang's[11] experiments in phase one.

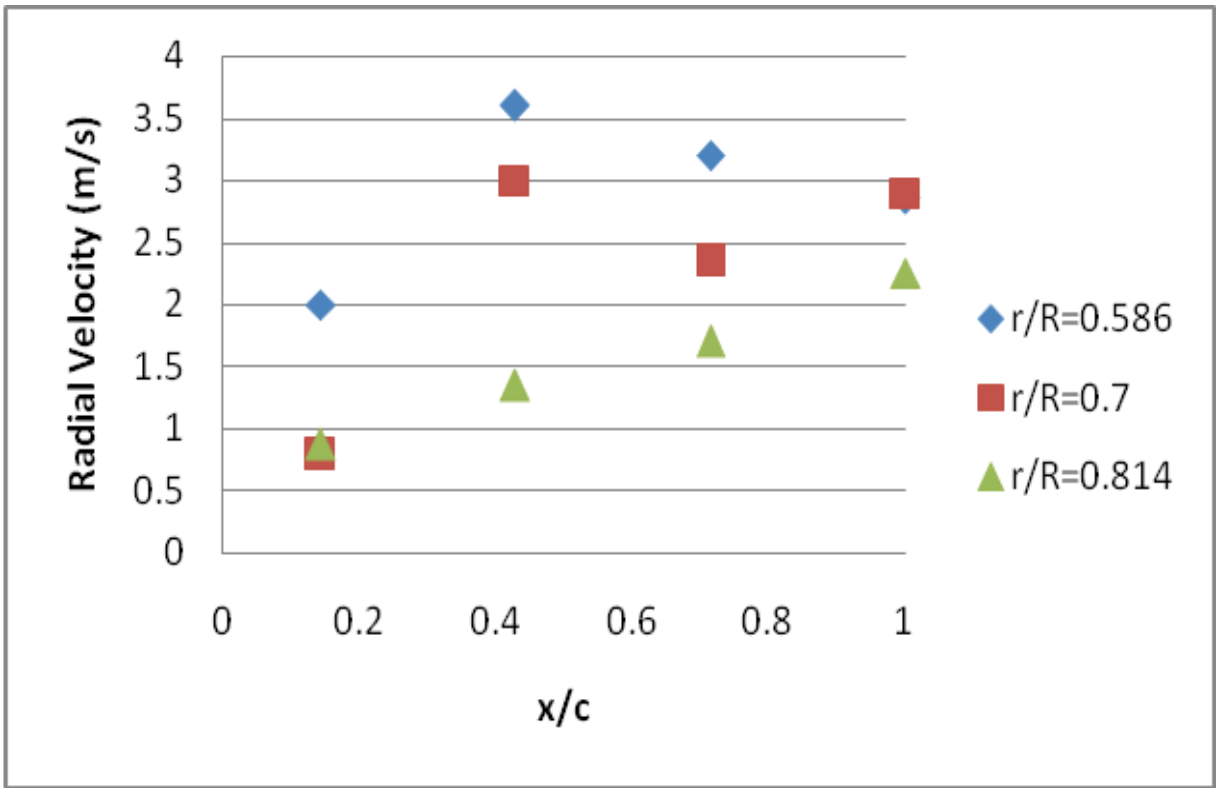

Figure 16 : Radial Velocity vs. Chorwise Location

Unlike those RMS results, the RMS profiles of all of the positions show the peak being close to the surface similar to the peak mean radial velocity. This suggests that all along the span and chord, the radial flow is a driver of instability. Additional analysis was done on the cells themselves. In each of the nine image positions in which cells appeared (three images forward of the separation point lacked structures), the diameter, cell *x* velocity, and cell *y* velocity was measured for thirty cells within the one hundred images. It is important to note that the cell *x* axis is parallel to the shaft axis; therefore, the cell *x* velocity will not be the same as blade radial velocity. An example of this cell data is shown in Figure 17. The triangles represent the average value while the line shows the standard deviation.

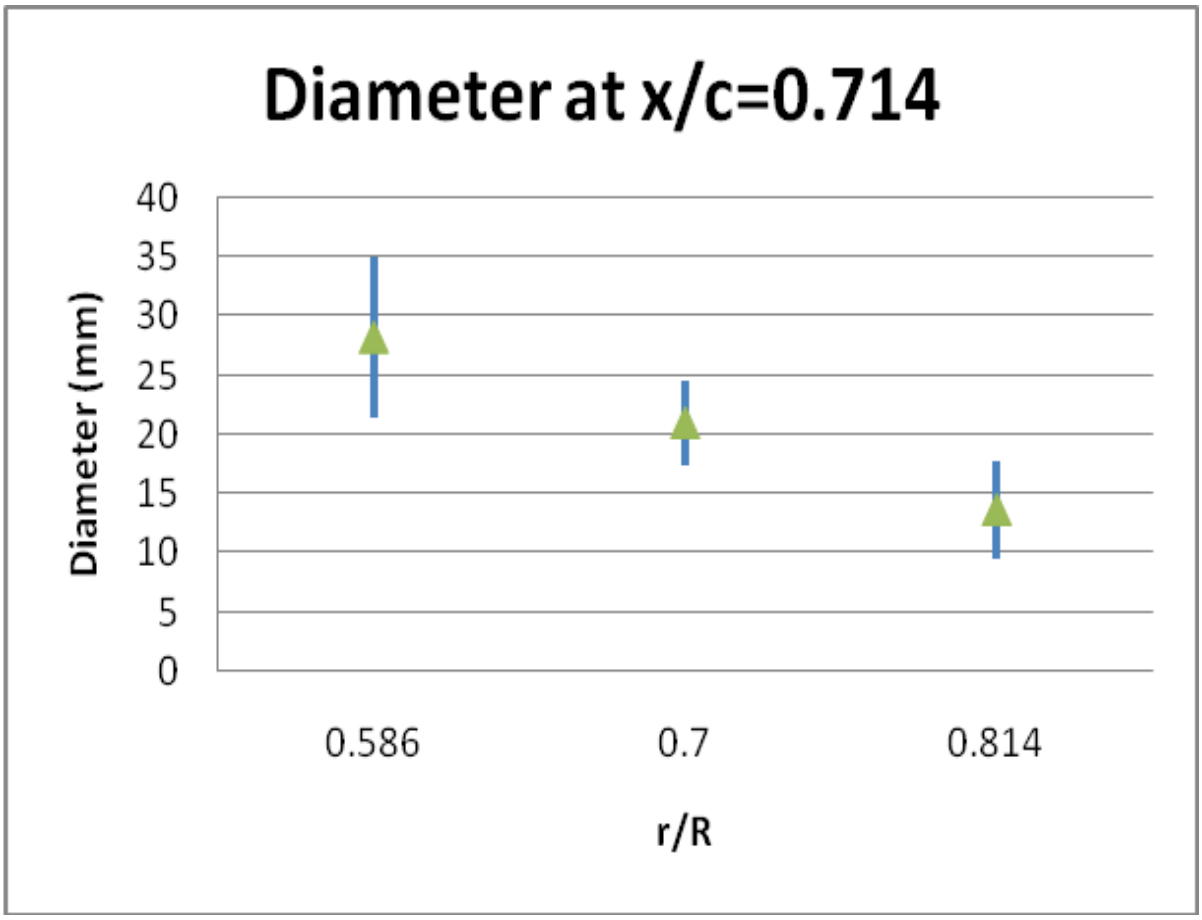

Figure 17 : Cell Diameter at x/c=0.714

Diameter, *x* velocity, and *y* velocity were analyzed along the span and along the chord. Cell diameter can be seen to decrease as you move outboard towards the tip and as you move from the trailing edge to the separation point. This supports that the cells are forming at the separation point and staying within the separated region, which grows as is progresses downstream of the blade. The change in *x* and *y* velocities give an idea of the strength of these structures along the span and chord. Most all of the spanwise and chordwise trends show an increase in magnitude of the downward *y* velocity within the cells. The *x* velocities at the different measurement locations show no clear trends along the span or chord. Additionally, the standard deviation is quite large, indicating a wide range of cell strength, with regard to *x* velocity, at different measurement points. In both cases however, the *x* and *y* velocities within the cells were higher than the flow around them.

CONCLUSIONS

1. A single-blade hover facility was used in the prior reporting period to study temporal evolution of flow close to a rotating blade. An inflow obstructor was validated as a means of inducing transient stall to simulate dynamic stall features downstream of the separation line.
2. PLIS and PIV verified occurrence of stall based on stoppage of through-flow.

3. Downstream of the stall line in the inflow obstructor case, radial velocity along the blade sharply develops an outward direction. However, the formation of stall cells along the radius exchanges fluid away from the blade boundary layer.
4. Time-varying cells of radial flow separation in the inflow obstructor case, comparable in scale to blade chord, occurred in the flowfield downstream of the stall line. These were not phase-locked to the rotor azimuth.
5. The same form of structures appears clearly in the forward flight dynamic stall flowfield studied during this reporting period in a wind tunnel rotor experiment. Co-rotating structures similar to a shear layer appear, and suggest that the free shear layer formed at stall, rolls up into discrete structures, or cells. However, actual upflow regions are not observed.
6. The spanwise spacing of structures is approximately the height of the separated flow region.
7. Radial velocity profiles show strong radial flow inboard, and weaker radial flow at outboard stations, corresponding to the expectation of deep stall inboard and attached flow near the tip.
8. The boundary layer under the radial flow is captured in the PIV data.
9. The radial flow profile appears to be fairly repeatable near the surface. However, above this region, the velocity profile is not repeatable from one cycle to another.
10. Moving upstream from the trailing edge to the separation line radial velocity does not vary substantially. Upstream of the separation point a decrease in outflow is observed which suggests that the inboard inflow begins to dominate.
11. RMS profiles prove that the radial flow is a driver of instability.
12. This, as far as we know, is the first capture and measurement of the quasi-periodic radial velocity field on a rotating blade, and in particular of the profile of the strong radial velocity above a rotating blade in stall.
13. The occurrence of discrete quasi-periodic but spatially repeatable vortical structures in this type of flow is also captured for the first time.

REFERENCES

1. Gregory, J., Sullivan J., Wanis, S., Komerath, N., "Pressure-sensitive paint as a distributed optical microphone array," Journal of the Acoustical Society of America, 119(1), 251-261, 2006
2. Yang, J., Balakrishnan, G., and Komerath, N.M, "Radial Flow Measurements Downstream of Forced Dynamic Separation on a Rotor Blade," 36th Fluid Dynamics Conference and Exhibit, AIAA, AIAA Paper 2006-3377, San Francisco, CA, June 2006.
3. DiOttavio, J., Watson, K., Cormey, J., Kondor, S. , Komerath, N., "Discrete Structures In The Radial Flow Over A Rotor Blade In Dynamic Stall". AIAA 2008-7344, Applied Aerodynamics Conference, August 2008.